Materials for Renewable and Sustainable Energy (2020) 9:5
https://doi.org/10.1007/s40243-020-0165-9

ORIGINAL PAPER

Suppression of magnetism and Seebeck effect in $Na_{0.875}CoO_2$ induced by Sb_{Co} dopants

M. H. N. Assadi[1] · Paolo Mele[2] · Marco Fronzi[3,4]

Received: 13 September 2019 / Accepted: 13 January 2020 / Published online: 21 January 2020

Abstract
We examined the electronic property of Sb-doped $Na_{0.785}CoO_2$ using density functional calculations based on GGA+U formalism. We demonstrated that Sb dopants were the most stable when replacing Co ions within the complex $Na_{0.875}CoO_2$ lattice structure. We also showed that the Sb_{Co} dopants adopted the +5 oxidation state introducing two electrons into the host $Na_{0.875}CoO_2$ compound. The newly introduced electrons recombined with holes that were borne on Co^{4+} sites that had been created by sodium vacancies. The elimination of Co^{4+} species, in turn, rendered $Na_{0.875}(Co_{0.9375}Sb_{0.0625})O_2$ non-magnetic and diminished the compound's thermoelectric effect. Furthermore, the Sb_{Co} dopants tended to aggregate with the Na vacancies keeping a minimum distance. The conclusions drawn here can be generalised to other highly oxidised dopants in Na_xCoO_2 that replace a Co.

Keywords Sodium cobaltate · Sb dopant · Thermoelectric effect · Magnetism · Density functional theory

Introduction

Sodium cobaltate (Na_xCoO_2) is an interesting and promising compound for high-efficiency thermoelectric material applications [1–3]. This compound also exhibits a rich magnetic and structural phase diagrams [4, 5]. Na_xCoO_2's unit cell consists of two alternating Na layers and edge-sharing CoO_6 octahedra. Co ions' mixed valency in Na deficient Na_xCoO_2 ($x<1$) creates a large spin entropy flow, and consequently, a large Seebeck coefficient [6]. Additionally, the Na layer in which Na^+ ions are amorphous and liquid like at room temperature [7] strongly scatters the heat-carrying phonons. The high mobility of Na ions leads to unprecedented freedom to favourably adjust all otherwise interdependent factors of the figure of merit (ZT) independently, giving Na_xCoO_2 an advantage over other thermoelectric materials [8, 9].

Controlling Na concentration (x) has been the primary technique to push the ZT of Na_xCoO_2 to higher limits [10]. However, given the volatile nature of Na ions, accurate experimental characterisation of Na concentration and its effect on the material's behaviour is somehow difficult [11]. This experimental difficulty motivated theoretical investigations into the structural and electronic properties of pristine Na_xCoO_2 [12–15]. Additionally, doping other elements in Na_xCoO_2 has also been utilised to improve sodium cobaltate's thermoelectric properties [16]. In spite of the efforts, doping Na_xCoO_2, as a strategy to enhance the thermoelectric performance, delivered mixed results. For instance, heavier ions such as rare earth Yb and noble metal Ag were successfully used to decrease the lattice thermal conductivity (k_l) and thus improving ZT [17, 18]. Doping Ru and Mn in $Na_{0.5}CoO_2$, however, increased the resistivity to ~ 300 μΩ m, three times higher than that of the undoped $Na_{0.5}CoO_2$ [19]. Similarly, co-doping Ti and Bi almost halved the Seebeck coefficient in $Na_{0.6}CoO_2$ to ~ 60 μK/V [20].

The mixed experimental results indicate that further progress in realising the functional applications of Na_xCoO_2 requires an accurate understanding of the effects of Na concentration and the presence of dopants on the electronic property of Na_xCoO_2. More specifically, the effect of the

✉ M. H. N. Assadi
h.assadi.2008@ieee.org

[1] School of Materials Science and Engineering, University of New South Wales, Sydney, NSW 2052, Australia

[2] Shibaura Institute of Technology, SIT Research Laboratories, 3-7-5, Toyosu, Koto-ku, Tokyo 135-8548, Japan

[3] International Research Centre for Renewable Energy, State Key Laboratory of Multiphase Flow in Power Engineering, Xian Jiaotong University, Xian 710049, China

[4] School of Mathematical and Physical Science, University of Technology Sydney, Sydney, NSW 2007, Australia

dopants on the delicate magnetic interactions in Na_xCoO_2 is still under debate [21] and needs careful investigation. In this work, therefore, the behaviour of Sb dopants in $Na_{0.875}CoO_2$ is examined using density functional theory. Na_xCoO_2 with higher Na concentration of $x \approx 0.8$, as considered here, possesses excessively higher Seebeck coefficient [22] and exhibits complex Na ordering patterns [5], thus is both appealing and challenging compound to explore. Our choice of Sb dopant was motivated by the successful synthesis of Sb-doped layered metal oxide compounds such as $LiMn_2O_4$/$LiSbO_3$ [23], $Na_3Ni_2SbO_6$ [24] and $Na_{3-x}Sn_{2-x}Sb_xNaO_6$ [25], all of which share considerable structural features with Na_xCoO_2. Furthermore, although the Sb-doped Na_1CoO_2, $Na_{0.75}CoO_2$ and $Na_{0.5}CoO_2$ compounds have been previously examined [26, 27], Sb doping in $Na_{0.875}CoO_2$, which is thermoelectrically more critical has not yet been explored in details.

Computational settings

Spin-polarised density functional calculations were performed with VASP package [28, 29] based on the projector augmented wave method [30, 31]. The energy cutoff was set to 500 eV. Generalised gradient approximation (GGA) [32, 33] was applied for the exchange–correlation functional. We added on-site Coulomb (U) and exchange (J) interaction terms of $U=5$ and $J=1$ eV to Co 3d electrons using Dudarev's approach [34]. Among many values reported for U and J in the literature [35–37], the chosen values reproduce the charge disproportionation [38, 39] of the Co ions more accurately. That is clearly distinguishing Co^{2+}, Co^{3+} and Co^{4+} from one another in terms of magnetisation and partial density of states. Furthermore, the value of $U_{eff}=4$ eV ($U_{eff}=U-J$) is at a midpoint between the low-end values of ~3 eV usually proposed for Co^{3+} [40] and the high-end values of ~5 eV proposed for Co^{4+} [41]. U_{eff} values close to 4 eV has been successfully applied to multivalent Co oxides [42, 43]. Brillouin zone sampling for the supercells was carried out by choosing a $4\times2\times2$ k-point set within the Monkhorst–Pack scheme [44]. We have successfully examined the convergence of these settings earlier [45, 46]. Charges localised on cationic centres were examined with Bader charge analysis code [47]. The quoted experimental ionic radii were compiled and reported by Shannon [48].

To obtain the $Na_{0.875}CoO_2$ supercell, we first optimised the $P6_3$/mmc unitcell of the Na_1CoO_2, which acts as the building block for the $Na_{0.875}CoO_2$ structure. The lattice parameters of a fully optimised primitive cell of Na_1CoO_2 were found to be 2.87 Å for a and 10.90 Å for c, which are in good agreement with the measurements [49]. Then two Na ions, one from each Na layer, were removed from the $2a\times4a\times1c$ Na_1CoO_2 supercell to construct the undoped $Na_{0.875}CoO_2$ structure. The most stable arrangement of the Na vacancies was adapted from our previous work [46], which is shown in Fig. 1. To obtain the final structures, the internal coordinates of all ions in the supercell were relaxed while the lattice constants were fixed to the calculated values of pristine Na_1CoO_2. The resulting $Na_{0.875}CoO_2$ unit cell had a primitive monoclinic ($P2$) representation in which all Na ions were at Na2 sites. Although the lattice parameters of $Na_{0.875}CoO_2$ were expected to be slightly different from those of Na_1CoO_2, dopants' formation energy is not significantly sensitive to this variation [12, 50]. For calculating Sb's formation energy, after dopant's placement in the $Na_{0.875}CoO_2$ structure, we fixed the lattice parameters of the doped supercell at the theoretical values of the pristine $Na_{0.875}CoO_2$, while all internal coordinates were relaxed. This procedure eliminates the artificial hydrostatic pressure ensuring that the final structures are in equilibrium [51, 52].

Results and discussion

We first have to consider the formation energy (E^f) of Sb dopants in Na_xCoO_2. Cationic Sb dopants can either replace a Co or be incorporated in the Na layer. Since Sb's ionic volume of 2.16×10^{-4} nm^3 is much larger than the interstitial

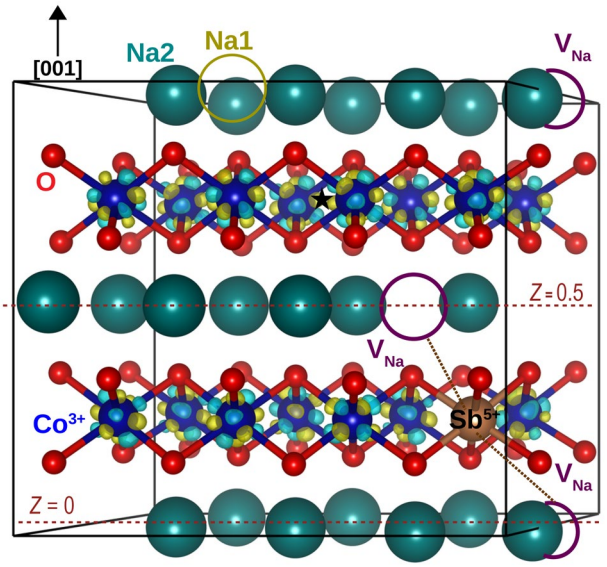

Fig. 1 The spin density of the $2a\times4a\times1c$ supercell used for simulating Sb-doped $Na_{0.875}CoO_2$ compound in the most stable configuration. Co and O ions occupy the Wyckoff $2a$ and $4f$ sites of the hexagonal lattice structure, respectively. In $Na_{0.875}CoO_2$, all Na ions occupy $2c$ (Na2) sites. For smaller Na concentrations, some Na ions occupy $2b$ (Na1) sites. The distance between V_{Na} and Sb^{5+} is marked with dotted brown lines. The spin density isosurfaces were drawn at $\rho=0.035$ e/Å^3. Yellow and cyan surfaces indicate spin-up and spin-down, respectively

cavity in CoO_6 layer of 1.79×10^{-7} nm^3 (marked with a star in Fig. 1), this interstitial site is too small for Sb doping. Furthermore, Sb in Na layer can either be substituted for a Na site (Na1 or Na2 as marked in Fig. 1) or be incorporated interstitially, e.g. occupying a vacant Na site. For $x=0.875$, Sb's formation energy has been reported earlier [26], using the standard supercell defect formation energy approach [53] and the triangular method for obtaining the chemical potentials [54]. The reported values belonged to an O rich environment in which Sb_3O_4 and CoO are the competing phases. The chemical potential (μ) for the oxygen-rich environment was set at $\mu_O=E^t(O_2)/2$ in which the $E^t(O_2)$ is the total energy of the O_2 molecule [55]. Accordingly, the most stable configuration was found Sb_{Co} with an E^f of 1.175 eV followed by Sb_{Na1} with an E^f of 4.547 eV, Sb_{Na2} with an E^f of 4.805 eV and finally Sb_{Int} with an E^f of 5.515 eV. This stability sequence is similar to that of Sb doping in Na_1CoO_2 ($x=1.00$) for which Sb_{Co} had an E^f of 1.356 eV while Sb_{Na1}, Sb_{Na2} and Sb_{Int} each had an E^f of 4.798 eV, 4.893 eV and 11.243 eV, respectively.

In the undoped $Na_{0.875}CoO_2$ compounds, Co^{4+} species are produced when the original Co^{3+} ions in the parent Na_1CoO_2 compound are oxidised to bear the holes created by V_{Na}s. As a result, the $Na_{14}Co_{16}O_{32}$ supercell of the $Na_{0.875}CoO_2$ compound has two holes borne on two Co^{4+} ions, one in each CoO_2 layer of the supercell. Sb dopants can adopt either +3 or +5 oxidation state. The Sb's partial density of states, as presented in Fig. 2, which corresponds to the configuration in Fig. 1, shows that both 5 s and 5p states are located above the Fermi level, indicating a +5 oxidation state. Since the supercell of the $Na_{0.875}CoO_2$:Sb_{Co} has a chemical composition of $Na_{14}Co_{15}Sb_1O_{32}$, charge neutrality implies that on average the oxidation state of Co ions is +3. In the most stable spin alignment, presented in Fig. 1, all Co ions have, indeed, an oxidation state of +3. Additionally, all Co ions were stabilised in the low spin configuration of $t_{2g}^6e_g^0$, further suggesting that this compound is non-magnetic. This is in contrast to the pristine $Na_{0.875}CoO_2$ compounds in which the Co^{4+} ions were antiferromagnetically aligned across the CoO_2 planes [56, 57]. Moreover, we have earlier shown that in Na_1CoO_2 and $Na_{0.75}CoO_2$, Sb_{Co} dopant also adopts the higher oxidation state [27].

The partial density of states of Sb_{Co}-doped $Na_{0.875}CoO_2$ [$Na_{0.875}(Co_{0.9375}Sb_{0.0625})O_2$], shown in Fig. 2, has some other noticeable features. Here, as expected [58, 59], under octahedral coordination, Co $3d_{z^2}$ and $3d_{x^2-y^2}$ orbitals directly overlap with O $2p_x$, $2p_y$, and $2p_z$ orbitals along the octahedral directions having σ hybridisation. This σ overlap results in low lying bonding e_g^b states with predominantly p character and high lying antibonding e_g^* states with predominantly d character. The remaining Co $3d_{xy}$, $3d_{xz}$, and $3d_{yz}$ orbitals point away from the O 2p orbitals and, therefore, have no

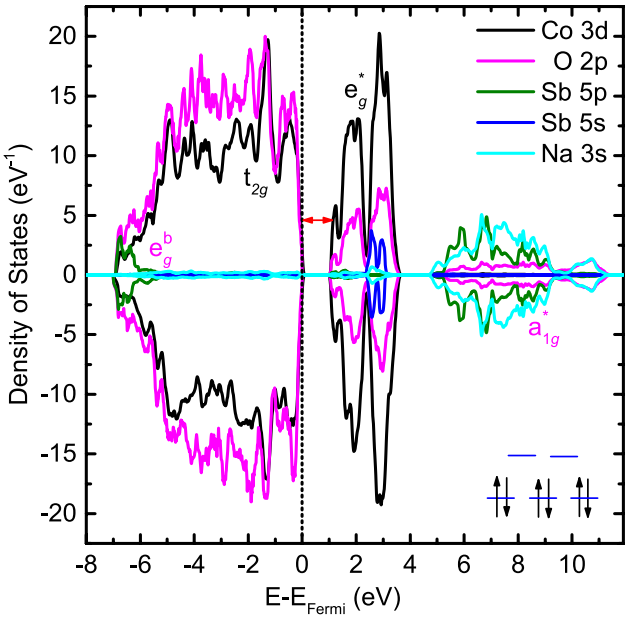

Fig. 2 The partial density of states (PDOS) of Sb_{Co}-doped $Na_{0.875}CoO_2$. The black and pink lines represent O 2p and Co's 3d PDOS, respectively while the blue and green lines represent Sb 5 s and 5p states, respectively. The cyan lines represent Na 3 s states. The electronic configuration of Co^{3+} is schematically shown in the inset at the bottom right corner

significant σ overlap with O 2p orbitals, constituting the nonbonding t_{2g} states. Moreover, the overlap of O 2p and Co 3p, and O 2p and Co 4 s orbitals form t_{1u}^* and a_{1g}^* bands, respectively, both of which located above the e_g^* states and have p character. Furthermore, there is a crystal field splitting of 1.01 eV (marked with a red arrow in Fig. 2) between the filled Co^{3+} t_{2g} states at the top of the valence band and the empty antibonding e_g states at the bottom of the conduction band forcing all Co^{3+} in the low spin state. The bandgap of 1.01 eV is smaller than that of Na_1CoO_2 (~2.2 eV) [45], indicating that Sb doping reduces the fundamental bandgap in $Na_{0.875}CoO_2$. Additionally, Sb's empty 5 s states are located at the top of the conduction band at ~2.5 eV hybridising with the empty e_g states while Sb's empty 5p states are located even higher at ~6 eV hybridising with the high lying Na's empty 3 s states. This arrangement is different from that of Sb^{5+} in Sb_2O_5 in which both Sb 5 s and 5p states are located within the same range at ~4 eV above Fermi level [60].

There is another possibility that the excess electrons introduced by Sb_{Co}' high oxidation state, instead of neutralising all hole introduced by V_{Na}s in Na deficient compounds, reduce the Co^{3+} species to Co^{2+} in $Na_{0.785}CoO_2$, while leaving all or some of the Co^{4+} ions unaltered. Co^{2+} and Co^{4+} are magnetic with a different spin and orbital degeneracies, implying that $Na_{0.875}CoO_2$: Sb_{Co} might potentially exhibit a

different magnetic and thermoelectric behaviour. We examined the possibility of alternative manifestation of oxidation states for Co ions in $Na_{0.875}CoO_2$: Sb_{Co} other than its most stable arrangement as presented in Fig. 1. In doing so, we constructed the alternative spin alignments by fixing the initial magnetic moment on the Co ions in the calculations. Several different configurations were considered of which a more stable spin bearing one is presented in Fig. 3. The partial density of Co ions with distinct oxidation and spin states are presented in Fig. 4. Here, we see that high spin Co^{4+} ($t_{2g}^3 e_g^2$) and low spin Co^{2+} ($t_{2g}^6 e_g^1$) species were both formed at the vicinity of Sb^{5+} dopant. Furthermore, a larger radius of Co^{2+} at octahedral coordination of 0.75 Å introduced significant lattice distortions that forced several Co^{3+} to take high spin configurations ($t_{2g}^4 e_g^2$). The total energy of this configuration was, however, higher than the non-magnetic configuration (Fig. 1) by 46.963 meV/Co, suggesting that Co ions in Sb-doped $Na_{0.875}CoO_2$ would be non-magnetic—all Co ions at $t_{2g}^6 e_g^0$ for a wide range of temperatures.

In Sb_{Co}-doped $Na_{0.875}CoO_2$ system [$Na_{0.875}(Co_{0.9375}Sb_{0.0625})O_2$], Sb dopants can occupy few distinct positions when substituting Co. For instance, either close to V_{Na}s, as shown in Fig. 1, which corresponds to the most stable arrangement of Sb dopant, or far from the V_{Na}s, as shown in Fig. 5. The distance between Sb_{Co} and V_{Na}s for the configuration presented in Fig. 1 is 2.23 Å for the V_{Na} at $Z=0$ and 2.23 Å for the V_{Na} at $Z=0.5$. These distances

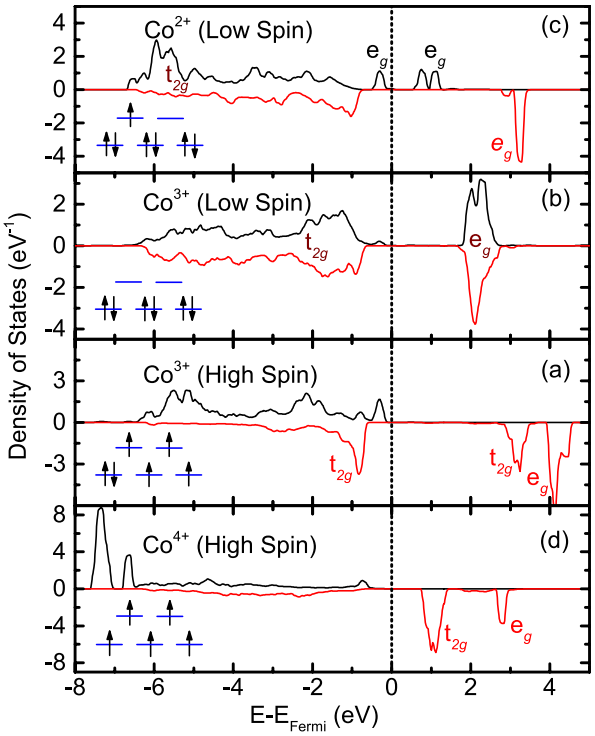

Fig. 4 The partial density of states of the Co 3d states of different oxidation states and spin states in the excited state presented in Fig. 3. Spin-up and spin-down channels are represented by black and red lines, respectively. The electronic configurations of various Co ions in the supercell are schematically shown in the insets at the bottom left corner

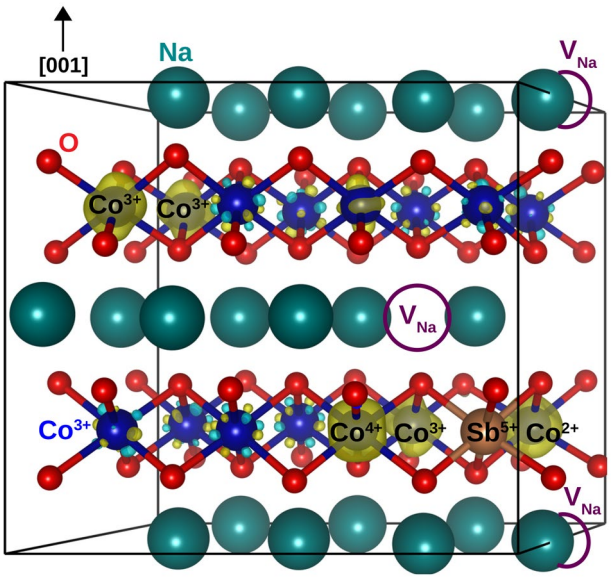

Fig. 3 The spin density of the $2a\times4a\times1c$ supercell used for simulating $Na_{0.875}CoO_2$:Sb_{Co} compound. Here, Sb^{5+} is at the closest distance to the V_{Na}s as in Fig. 1, however, the spin state of Co ions corresponds to an excited state

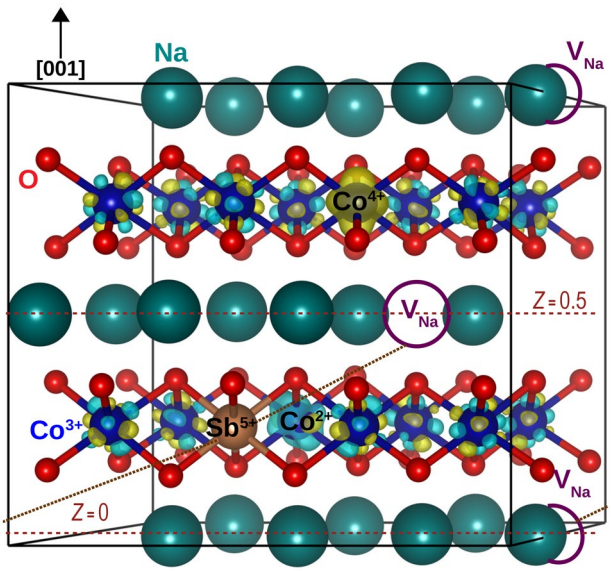

Fig. 5 The spin density of the $2a\times4a\times1c$ supercell used for simulating Sb-doped $Na_{0.875}CoO_2$ compound when Sb^{5+} is not in the immediate vicinity of the V_{Na}s. The distance between V_{Na} and Sb^{5+} is marked with dotted brown lines

for the configuration presented in Fig. 5 were 5.23 Å for the V_{Na} at $Z=0$ and 5.26 Å for the V_{Na} at $Z=0.5$. We found the total energy of the configuration in Fig. 1 was 27.620 meV/Co lower, and hence more stable than the configuration in Fig. 5. One possible explanation for the aggregation of Sb dopant and the V_{Na}s is that the radius of Sb^{5+} in octahedral coordination (0.60 Å) is ~ 8.3% larger than that of Co^{3+} (0.55 Å). As a consequence, the location of larger Sb ion in the vicinity of V_{Na} results in the cancellation of internal lattice stress leading to greater stability.

In the case where the $Sb^{5+}_{Co^{3+}}$ dopant is far away from the V_{Na}s as in Fig. 5, unlike the case of the ground state in Fig. 1, the electrons of the Sb^{5+} do not neutralise both of the holes that are borne on the Co^{4+} ions in the supercell. As shown in Fig. 5, only the Co^{4+} at the bottom CoO_2 layer which contains the $Sb^{5+}_{Co^{3+}}$ dopant has been reduced to Co^{3+} while the Co^{4+} in the top layer has remained unaltered. The extra electron of the Sb dopant, instead, reduces a Co^{3+} in the vicinity of the Sb dopant to Co^{2+}. Since the Co^{4+} ions are located near the V_{Na}s in the undoped compound [45], doping $Sb^{5+}_{Co^{3+}}$ in the vicinity of V_{Na}s (as in Fig. 1), facilitates the charge transfer from Sb to two cationic nearest neighbour Co^{4+} ions. However, when the $Sb^{5+}_{Co^{3+}}$ is far away from the V_{Na}s, as in Fig. 5, there is no cationic nearest neighbour charge transfer possible between Sb and Co^{4+} at the top layer. Consequently, the extra electron of $Sb^{5+}_{Co^{3+}}$ is localised on a neighbouring Co^{3+} in the bottom layer converting it to Co^{2+}. We verified the stability of this spin alignment for the configuration in Fig. 5 by fixing the spin of all Co to zero ($t_{2g}^6 e_g^0$) which resulted in a 112.6 meV/Co higher total energy.

In Na_xCoO_2, the Seebeck effect is facilitated by the spin entropy transfer between Co^{3+} and Co^{4+} ions for which the Seebeck coefficient can be estimated by the modified Heikes formula [61, 62]:

$$S(T \to \infty) = -\frac{k_B}{e}\mathrm{Ln}\left(\frac{g\left(Co^{3+}\right)}{g\left(Co^{4+}\right)} \cdot \frac{\rho}{1-\rho}\right), \quad (1)$$

in which k_B and e are the Boltzmann constant and electron's charge, respectively. $g(Co^{3+})$ and $g(Co^{4+})$ are the electronic degeneracies of Co^{3+} and Co^{4+} ions, respectively, and ρ is the hole concentration. The electronic degeneracies are calculated by multiplying the orbital ($g_{orbital}$) and spin (g_{spin}) degeneracies of electrons for a given transition metal ion. In low spin, octahedral coordination for which Co^{3+} and Co^{4+} electrons occupy t_{2g} orbitals only, $g_{orbital}$ is the total number of permutation of electrons and is calculated as:

$$g_{\mathrm{orbital}} = \frac{3!}{n^{\uparrow}!(3-n^{\uparrow})!} \cdot \frac{3!}{n^{\downarrow}!(3-n^{\downarrow})!}, \quad (2)$$

in which $n^{\uparrow}$ and $n_{\downarrow}$ are the number of spin-up and spin-down electrons, respectively. g_{spin}, on the other hand, equals to $2\xi+1$, where ξ is the total spin number of a given ion. Plugging the values for Co^{3+} and Co^{4+} renders $g(Co^{3+})=1$ and $g(Co^{4+})=6$. Additionally, since conduction in $Na_{0.875}CoO_2$ is achieved by holes hopping form a Co^{4+} site to a Co^{3+} site, the hole concentration is proportional to the ratio of Co^{4+} site to the total Co sites. Consequently, $S(T\to\infty)=322.08$ μK/V in pristine $Na_{0.875}CoO_2$. Equation 1 establishes a reverse relationship between ρ and S; so that for raising the Seebeck coefficient, one must reduce the concentration of Co^{4+} species [63].

The introduction of one Sb_{Co} dopant into the $Na_{14}Co_{16}O_{32}$ supercell, however, eliminates the Co^{4+} species and brings the hole concentration to zero resulting in a band insulating character for $Na_{0.875}CoO_2$:Sb_{Co}. This is inferable from the partial density of states in Fig. 2, which shows a bandgap of 1.01 eV. As a consequence, according to Eq. 1, the Seebeck coefficient diverges. Experimentally, however, Seebeck effect measurements in insulators have indicated that the Seebeck potential approaches zero as carrier concentration diminishes [64]. Mahan has attributed this apparent contradiction to the fact that the Seebeck potential does not diminish but rather a space-charge effect in insulators screens off the Seebeck potential [65, 66]. In any case, in the absence of any carriers, $Na_{0.875}CoO_2$:Sb_{Co} is of no use for converting heat gradient to measurable electric energy. Although reducing the concentration of Co^{4+} increases S, in choosing the dopant and its concentration for Na_xCoO_2, one, nonetheless, must apply due diligence to avoid the catastrophic complete electron–hole recombination.

It is quite instructive to know that several times, similar to the case of $Na_{0.875}CoO_2$: Sb_{Co}, ineffective doping cases on thermoelectric compounds have been reported in the literature. For example, Al doping plays no effect on $Mg_2Si_{0.75}Sn_{0.25}$ [67]. In Ni-doped $CuInTe_2$ Ni-doping is rather ineffective regarding the increase of the hole concentration and the decrease of the thermal conductivity [68]. In Mg_3Sb_2, interstitial doping with Li, Zn, Cu, and Be is found to be ineffective for n-type doping; however, Li is identified as a good p-type dopant [69]. Bi is an ineffective dopant in Mg_2Ge and precipitates into Mg_2Bi_3 [70]. Boron is ineffective as dopant in α-MgAgSb [71].

Conclusions

In this work, using density functional theory, the formation energy of Sb dopants in $Na_{0.875}CoO_2$ was examined. The main findings of this investigation can be summarised as follow: (1) Sb_{Co} is the most stable configuration $Na_{0.875}CoO_2$ as it is in Na_1CoO_2 as well. This trend is similar to the Sb dopant in other sodium cobaltates with smaller Na concentrations [26, 27]. Moreover, as x increases the margin of the stabilisation of Sb_{Co} configuration increases

against those other configurations in which Sb is located in the Na layer; (2) the formation energy of Sb_{Co} decreases with decreasing x—$E^f(Na_1CoO_2{:}Sb_{Co}) = 1.356$ eV and $E^f(Na_{0.875}CoO_2{:}Sb_{Co}) = 1.175$ eV. This trend implies that doping Na deficient systems with Sb is practically easier; (3) in $Na_{0.875}CoO_2{:}Sb_{Co}$, Sb's 5 s states are located above the Fermi level hybridising with Co's empty e_g states while Sb's 5p states are located even higher along with Na's 3 s states implying an oxidation state of 5 + for Sb_{Co}; (4) in $Na_{0.875}CoO_2{:}Sb_{Co}$, Sb_{Co} tends to aggregate with the V_{Na}s; (5) in the most stable configuration, Sb dopants reduce the magnetic Co^{4+} ion to non-magnetic Co^{3+} abating both the long-range magnetic order and the Seebeck effect which is sustained by spin entropy flow in undoped Na_xCoO_2; (6) in an excited state, in $Na_{0.875}CoO_2{:}Sb_{Co}$, a pair of non-magnetic Co^{3+} can be transformed into magnetic Co^{2+} and Co^{4+}. Such magnetic state is, however, higher in energy by 46.963 meV/Co than the non-magnetic ground state. Finally, we demonstrated how a generally favourable strategy such as reducing carrier concentration for increasing the Seebeck coefficient can suppress the Seebeck effect for a specific dopant and Na concentrations in Na_xCoO_2.

Acknowledgements This work was supported by the Australian Research Council. The simulation facility was provided by Australian National Computational Infrastructure and Intersect Ltd.

References

1. Fergus, J.W.: Oxide materials for high temperature thermoelectric energy conversion. J. Eur. Ceram. Soc. **32**, 525–540 (2012)
2. Ravichandran, J.: Thermoelectric and thermal transport properties of complex oxide thin films, heterostructures and superlattices. J. Mater. Res. **32**, 183–203 (2016)
3. Matsuno, J., Fujioka, J., Okuda, T., Ueno, K., Mizokawa, T., Katsufuji, T.: Strongly correlated oxides for energy harvesting. Sci. Technol. Adv. Mater. **19**, 899–908 (2018)
4. Mendels, P., Bono, D., Bobroff, J., Collin, G., Colson, D., Blanchard, N., Alloul, H., Mukhamedshin, I., Bert, F., Amato, A.: Cascade of bulk magnetic phase transitions in Na_xCoO_2 as studied by muon spin rotation. Phys. Rev. Lett. **94**, 136403 (2005)
5. Berthelot, R., Carlier, D., Delmas, C.: Electrochemical investigation of the P2–Na_xCoO_2 phase diagram. Nat. Mater. **10**, 74–80 (2011)
6. Chen, S.-D., He, Y., Zong, A., Zhang, Y., Hashimoto, M., Zhang, B.-B., Yao, S.-H., Chen, Y.-B., Zhou, J., Chen, Y.-F., Mo, S.-K., Hussain, Z., Lu, D., Shen, Z.-X.: Large thermopower from dressed quasiparticles in the layered cobaltates and rhodates. Phys. Rev. B **96**, 081109 (2017)
7. Zhang, W., Zhu, K., Liu, J., Wang, J., Yan, K., Liu, P., Wang, Y.: Influence of the phase transformation in Na_xCoO_2 ceramics on thermoelectric properties. Ceram. Int. **44**, 17251–17257 (2018)
8. Snyder, G.J., Toberer, E.S.: Complex thermoelectric materials. Nat. Mater. **7**, 105–114 (2008)
9. Voneshen, D., Refson, K., Borissenko, E., Krisch, M., Bosak, A., Piovano, A., Cemal, E., Enderle, M., Gutmann, M., Hoesch, M.: Suppression of thermal conductivity by rattling modes in thermoelectric sodium cobaltate. Nat. Mater. **12**, 1028–1032 (2013)
10. Luo, J., Wang, N., Liu, G., Wu, D., Jing, X., Hu, F., Xiang, T.: Metamagnetic transition in $Na_{0.85}CoO_2$ single crystals. Phys. Rev. Lett. **93**, 187203 (2004)
11. Cushing, B.L., Wiley, J.B.: Improved synthetic routes to layered Na_xCoO_2 oxides. Synth. React. Inorg. Met. Chem. **29**, 1199–1207 (1999)
12. Zhang, P., Capaz, R.B., Cohen, M.L., Louie, S.G.: Theory of sodium ordering in Na_xCoO_2. Phys. Rev. B **71**, 153102 (2005)
13. Meng, Y.S., Hinuma, Y., Ceder, G.: An investigation of the sodium patterning in Na_xCoO_2 (0.5%3c x%3c 1) by density functional theory methods. J. Chem. Phys. **128**, 104708 (2008)
14. Wang, Y., Ni, J.: Ground state structure of sodium ions in Na_xCoO_2: a combined Monte Carlo and first-principles approach. Phys. Rev. B **76**, 094101 (2007)
15. Wang, G.-T., Dai, X., Fang, Z.: Phase diagram of Na_xCoO_2 studied by Gutzwiller density-functional theory. Phys. Rev. Lett. **101**, 066403 (2008)
16. Richter, R., Shopova, D., Xie, W., Weidenkaff, A., Lechermann, F.: Thermopower enhancement from engineering the $Na_{0.7}CoO_2$ interacting fermiology via Fe doping. Adv. Cond. Matter. Phys. **18**, 1–7 (2018)
17. Nagira, T., Ito, M., Hara, S.: Effect of partial substitutions of rare-earth metals for Na-site on the thermoelectric properties of $Na_xCo_2O_4$ prepared by the polymerized complex method. Mater. Trans. **45**, 1339–1345 (2004)
18. Seetawan, T., Amornkitbamrung, V., Burinprakhon, T., Maensiri, S., Kurosaki, K., Muta, H., Uno, M., Yamanaka, S.: Thermoelectric power and electrical resistivity of Ag-doped $Na_{1.5}Co_2O_4$. J. Alloys Compd. **407**, 314–317 (2006)
19. Li, S., Funahashi, R., Matsubara, I., Sodeoka, S.: Magnetic and thermoelectric properties of $NaCo_{2-x}M_xO_4$ (M = Mn, Ru). Mater. Res. Bull. **35**, 2371–2378 (2000)
20. Buntham, S., Keawprak, N., Watcharapasorn, A.: Thermoelectric and magnetic properties of $Bi_{0.5}Na_{0.5}TiO_3$-doped Na_xCoO_2 ceramics. J. Nanosci. Nanotechnol. **17**, 3439–3442 (2017)
21. Mandal, P.: Anomalous transport properties of Co-site impurity doped Na_xCoO_2. J. Appl. Phys. **104**, 063902 (2008)
22. Terasaki, I., Sasago, Y., Uchinokura, K.: Large thermoelectric power in $NaCo_2O_4$ single crystals. Phys. Rev. B **56**, R12685–R12687 (1997)
23. Cui, P., Liang, Y., Zhan, D., Zhao, Y., Peng, R.: Study on the preparation and characteristics of the Li–Mn–Sb–O nanocomposite as a cathode material for Li-ion batteries. RSC Adv. **4**, 43821–43827 (2014)
24. Yuan, D., Liang, X., Wu, L., Cao, Y., Ai, X., Feng, J., Yang, H.: A Honeycomb-Layered $Na_3Ni_2SbO_6$: a high-rate and cycle-stable cathode for sodium-ion batteries. Adv. Mater. **26**, 6301–6306 (2014)
25. Smaha, R.W., Roudebush, J.H., Herb, J.T., Seibel, E.M., Krizan, J.W., Fox, G.M., Huang, Q., Arnold, C.B., Cava, R.J.: Tuning sodium ion conductivity in the layered honeycomb oxide $Na_{3-x}Sn_{2-x}Sb_xNaO_6$. Inorg. Chem. **54**, 7985–7991 (2015)

26. Assadi, M.H.N., Katayama-Yoshida, H.: Dopant incorporation site in sodium cobaltate's host lattice: a critical factor for thermoelectric performance. J. Phys. Condens. Matter. **27**, 175504 (2015)
27. Assadi, M.H.N., Li, S., Zheng, R.K., Ringer, S.P., Yu, A.B.: Magnetic, electrochemical and thermoelectric properties of P2-$Na_x(Co_{7/8}Sb_{1/8})O_2$. Chem. Phys. Lett. **687**, 233–237 (2017)
28. Kresse, G., Furthmüller, J.: Efficient iterative schemes for ab initio total-energy calculations using a plane-wave basis set. Phys. Rev. B **54**, 11169 (1996)
29. Kresse, G., Furthmüller, J.: Efficiency of ab-initio total energy calculations for metals and semiconductors using a plane-wave basis set. Comput. Mater. Sci. **6**, 15–50 (1996)
30. Blöchl, P.E.: Projector augmented-wave method. Phys. Rev. B **50**, 17953–17979 (1994)
31. Kresse, G., Joubert, D.: From ultrasoft pseudopotentials to the projector augmented-wave method. Phys. Rev. B **59**, 1758–1775 (1999)
32. Perdew, J.P., Burke, K., Ernzerhof, M.: Generalized gradient approximation made simple. Phys. Rev. Lett. **77**, 3865–3868 (1996)
33. Perdew, J.P., Burke, K., Ernzerhof, M.: Generalized gradient approximation made simple errata. Phys. Rev. Lett. **78**, 1396–1396 (1997)
34. Dudarev, S., Botton, G., Savrasov, S., Humphreys, C., Sutton, A.: Electron-energy-loss spectra and the structural stability of nickel oxide: an LSDA+U study. Phys. Rev. B **57**, 1505–1509 (1998)
35. Lee, K.W., Pickett, W.: Charge and spin ordering in insulating $Na_{0.5}CoO_2$: effects of correlation and symmetry. Phys. Rev. Lett. **96**, 096403 (2006)
36. Hinuma, Y., Meng, Y.S., Ceder, G.: Temperature-concentration phase diagram of P_2-Na_xCoO_2 from first-principles calculations. Phys. Rev. B **77**, 224111 (2008)
37. Molenda, J., Baster, D., Molenda, M., Świerczek, K., Tobola, J.: Anomaly in the electronic structure of the Na_xCoO_{2-y} cathode as a source of its step-like discharge curve. Phys. Chem. Chem. Phys. **16**, 14845–14857 (2014)
38. Mukhamedshin, I., Alloul, H.: Na order and Co charge disproportionation in Na_xCoO_2. Phys. B **460**, 58–63 (2015)
39. Mukhamedshin, I., Dooglav, A., Krivenko, S., Alloul, H.: Evolution of Co charge disproportionation with Na order in Na_xCoO_2. Phys. Rev. B **90**, 115151 (2014)
40. Jain, A., Hautier, G., Ong, S.P., Moore, C.J., Fischer, C.C., Persson, K.A., Ceder, G.: Formation enthalpies by mixing GGA and GGA+ U calculations. Phys. Rev. B **84**, 045115 (2011)
41. Aykol, M., Wolverton, C.: Local environment dependent GGA+*U* method for accurate thermochemistry of transition metal compounds. Phys. Rev. B **90**, 115105 (2014)
42. Aykol, M., Kim, S., Wolverton, C.: van der waals interactions in layered lithium cobalt oxides. J. Phys. Chem. C **119**, 19053–19058 (2015)
43. Zhao, Z., Yao, J., Sun, B., Zhong, S., Lei, X., Xu, B., Ouyang, C.: First-principles identification of spinel $CaCo_2O_4$ as a promising cathode material for Ca-ion batteries. Solid State Ion. **326**, 145–149 (2018)
44. Monkhorst, H.J., Pack, J.D.: Special points for Brillouin-zone integrations. Phys. Rev. B **13**, 5188–5192 (1976)
45. Assadi, M.H.N., Katayama-Yoshida, H.: Interplay between Magnetism and Na concentration in Na_xCoO_2. Funct. Mater. Lett. **08**, 1540016 (2015)
46. Assadi, M.H.N., Katayama-Yoshida, H.: Magnetism and spin entropy in Ru doped $Na_{0.5}CoO_2$. Phys. Chem. Chem. Phys. **19**, 23425–23430 (2017)
47. Yu, M., Trinkle, D.R.: Accurate and efficient algorithm for Bader charge integration. J. Chem. Phys. **134**, 064111 (2011)
48. Shannon, R.D.: Revised effective ionic radii and systematic studies of interatomic distances in halides and chalcogenides. Acta Crystallogr. A **32**, 751–767 (1976)
49. Chen, D., Chen, H., Maljuk, A., Kulakov, A., Zhang, H., Lemmens, P., Lin, C.: Single-crystal growth and investigation of Na_xCoO_2 and $N_xCoO_2{\cdot}y\ H_2O$. Phys. Rev. B **70**, 024506 (2004)
50. Geck, J., Zimmermann, M.V., Berger, H., Borisenko, S.V., Eschrig, H., Koepernik, K., Knupfer, M., Büchner, B.: Stripe correlations in $Na_{0.75}CoO_2$. Phys. Rev. Lett. **97**, 106403 (2006)
51. Lany, S., Zunger, A.: Accurate prediction of defect properties in density functional supercell calculations. Model. Simul. Mater. Sci. Eng. **17**, 084002 (2009)
52. Fratesi, G.: First-principles investigation of the early stages of Pd adsorption on Au (111). J. Phys. Condens. Matter. **23**, 015001 (2010)
53. Freysoldt, C., Grabowski, B., Hickel, T., Neugebauer, J., Kresse, G., Janotti, A., Van de Walle, C.G.: First-principles calculations for point defects in solids. Rev. Mod. Phys. **86**, 253–305 (2014)
54. Hoang, K.: First-principles theory of doping in layered oxide electrode materials. Phys. Rev. Mater. **1**, 075403 (2017)
55. Long, R., English, N.J.: Electronic properties of F/Zr co-doped anatase TiO_2 photocatalysts from GGA+U calculations. Chem. Phys. Lett. **498**, 338–344 (2010)
56. Bayrakci, S., Mirebeau, I., Bourges, P., Sidis, Y., Enderle, M., Mesot, J., Chen, D., Lin, C., Keimer, B.: Magnetic ordering and spin waves in $Na_{0.82}CoO_2$. Phys. Rev. Lett. **94**, 157205 (2005)
57. Alloul, H., Mukhamedshin, I.R., Dooglav, A.V., Dmitriev, Y.V., Ciomaga, V.C., Pinsard-Gaudart, L., Collin, G.: ^{23}Na NMR study of sodium order in Na_xCoO_2 with 22 K Neel temperature. Phys. Rev. B **85**, 134433 (2012)
58. Aydinol, M.K., Kohan, A.F., Ceder, G., Cho, K., Joannopoulos, J.: Ab initio study of lithium intercalation in metal oxides and metal dichalcogenides. Phys. Rev. B **56**, 1354–1365 (1997)
59. Assadi, M.H., Hussein, N., Fronzi, M., Ford, M., Shigeta, Y.: High-performance Na ion cathodes based on the ubiquitous and reversible O redox reaction. J. Mater. Chem. A **6**, 24120–24127 (2018)
60. Allen, J.P., Carey, J.J., Walsh, A., Scanlon, D.O., Watson, G.W.: Electronic structures of antimony oxides. J. Phys. Chem. C **117**, 14759–14769 (2013)
61. Koshibae, W., Tsutsui, K., Maekawa, S.: Thermopower in cobalt oxides. Phys. Rev. B **62**, 6869–6872 (2000)
62. Nag, A., Shubha, V.: Oxide thermoelectric materials: a structure-property relationship. J. Electron. Mater. **43**, 962–977 (2014)
63. Assadi, M.H.N.: Na site doping a pathway for enhanced thermoelectric performance in $Na_{1-x}CoO_2$: the case of Gd and Yb dopants. J. Phys. Condens. Matter. **32,** 125502 (2020). https://doi.org/10.1088/1361-648X/ab5bdb
64. Bentien, A., Johnsen, S., Madsen, G., Iversen, B., Steglich, F.: Colossal Seebeck coefficient in strongly correlated semiconductor $FeSb_2$. EPL **80**, 17008 (2007)
65. Mahan, G.D.: The low-temperature seebeck coefficient in insulators. J. Electron. Mater. **44**, 431–434 (2015)
66. Mahan, G.D.: The seebeck coefficient of insulators: electrochemical potential. J. Electron. Mater. **45**, 1257–1259 (2016)
67. Isoda, Y., Held, M., Tada, S., Shinohara, Y.: Effects of Al/Sb double doping on the thermoelectric properties of $Mg_2Si_{0.75}Sn_{0.25}$. J. Electron. Mater. **43**, 2053–2058 (2014)
68. Kucek, V., Drasar, C., Navratil, J., Plechacek, T., Benes, L.: Thermoelectric properties of Ni-doped $CuInTe_2$. J. Phys. Chem. Solids **83**, 18–23 (2015)
69. Gorai, P., Ortiz, B.R., Toberer, E.S., Stevanović, V.: Investigation of n-type doping strategies for Mg_3Sb_2. J. Mater. Chem. A **6**, 13806–13815 (2018)
70. Santos, R., Dou, S.X., Vashaee, D., Aminorroaya, Y.S.: Effect of the fabrication technique on the thermoelectric performance

of Mg-based compounds. A case study of n-type Mg2Ge. ACS Omega **2**, 8069–8074 (2017)
71. Gao, W., Yi, X., Cui, B., Wang, Z., Huang, J., Sui, J., Liu, Z.: The critical role of boron doping in the thermoelectric and mechanical properties of nanostructured α-MgAgSb. J. Mater. Chem. C **6**, 9821–9827 (2018)